J Wood Sci (1999) 45:134–142

ORIGINAL ARTICLE

Zhi-Hui Wu · Takeshi Furuno

Stress distributions and failure types of curved laminated veneer lumber for use in furniture under loading*

Received: June 19, 1998 / Accepted: August 18, 1998

Abstract To control reliably the suitable use of curved laminated veneer lumber (LVL) as a structural member of furniture, stress distributions and failure types of curved LVL made from massion pine (*Pinus massoniana* Lamb.) and fast-growing poplar (*Populus euramericana* CV. I.) were investigated under end-pull, end-thrust, and transverse loading. The results are summarized as follows: In curved LVL of two wood species, absolute values of the maximum axial stress (σ_A) occurring at the convex surface are smaller than those (σ_B) that occurred at the concave surface. The differences between these values decrease with an increase in the radius of curvature. With end-pull loading, there were mainly splitting failures at glue lines near the centroidal axis. With end-thrust loading, there were more fibrous fractures on the tensile side and crushing failures on the compression side. With transverse loading, curved specimens of massion pine exhibited mainly splitting failures. In contrast, for curved LVL of fast-growing poplar, fibrous fractures occurred mainly on the tensile side. Absolute values of $\sigma_A$and σ_B significantly increased with an increase in the radius of curvature. In contrast, absolute values of the maximum radial stress (σ_R) decreased with an increase in the radius of curvature. Absolute values of σ_A, σ_B, and σ_R of curved LVL of massion pine were larger under end-thrust loading than under end-pull and transverse loading. Conversely, absolute values of σ_A and σ_B of curved LVL of fast-growing poplar were small under end-thrust loading. However, absolute values of σ_A and σ_B of curved LVL of two wood species under end-pull loading were almost similar to those under transverse loading.

Key words Fast-growing species · Curved LVL · Load · Stress · Failure type

Z.-H. Wu · T. Furuno (✉)
Faculty of Science and Engineering, Shimane University, Matsue 690-8504, Japan
Tel. +81-852-32-6563; Fax +81-852-32-6123
e-mail: t-furuno@riko.shimane-u.ac.jp

Z.-H. Wu
College of Wood Science and Technology, Nanjing Forestry University, Nanjing 210037, China

*Part of this study was presented at the 10th annual meeting of Chugoku Shikoku branch of the Japan Wood Research Society, Miki, Kagawa, September 25, 1998 and the 4th Pacific Rim Bio-Based Composites Symposium, Bogor, Indonesia, November 2–5, 1998

Introduction

Curved laminated veneer lumber (LVL) was produced from veneers using a bending and gluing operation. Glue-coated pieces of veneer were assembled and pressed between molds; and pressure and heat were applied until gluelines set and finally held an assembly to the desired curved shape with a small radius of curvature. Curved LVL can provide a variety of functional and aesthetically pleasing wood members for furniture such as chairs, sofas, and tables.[1–3]

To control reliably the suitable use of curved LVL in structural member of furniture, in this study experimental specimens of curved LVL made from two fast-growing wood species [massion pine (*Pinus massoniana* Lamb.) and fast-growing poplar (*Populus euramericana* CV. I.)] were tested under loading. There are mainly three conditions of loading for curved LVL: end-pull, end-thrust, and transverse. These conditions of loading were applied to curved specimens.[4–14] The condition applied to straight specimens only was transverse loading. Firstly, the maximum fracture loads and failure types of the curved and straight specimens were tested and observed under different conditions of loading. Then, according to the theory of the strength of materials, the axial stress (a combination of normal stress and bending stress) and radial stress of these specimens in loading tests were calculated.[4–14] To obtain suitable conditions of loading on curved LVL, the effects of the radius of curvature and the condition of loading on stress distributions and failure types of curved LVL were analyzed.

Theory

End-pull loading (bending)

When the pull load P that increased the radius of curvature and caused the curved LVL to become straighter is imposed at two ends of curved specimens with a span of L, shown in Fig. 1a, the bending moment M is negative, by convention, because it subjects the curved member to increase the radius of curvature. A positive bending moment induces opposite effects.[8,12] M is represented as

$$M = -P\left(H + \frac{h}{2}\right) \tag{1}$$

where H is the distance between the concave and the line of the loading or support points, and h is the thickness of the curved specimens.

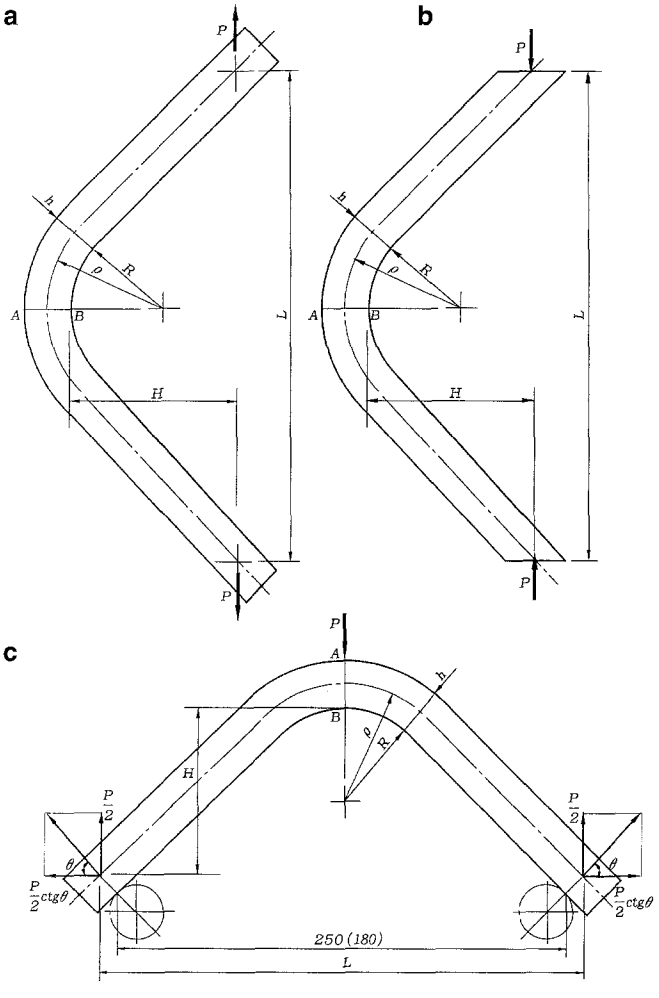

Fig. 1. Conditions of loading of curved laminated veneer lumber (LVL). **a** End-pull loading, **b** End-thrust loading, **c** Transverse loading. R, ϱ, radius of curvature of the concave surface and centroidal axis; h, thickness; H, distance between the concave side and the line of the loading or support points; L, support or imposition span; P, maximum load; θ, support angle on horizon under transverse loading

As shown in Fig. 2, the normal stress σ_0 (tensile stress) in the axis at the throughout cross section can be given as

$$\sigma_0 = \frac{P}{bh} \tag{2}$$

where b is the width of the curved specimens.

The bending stress σ_b in the axis throughout the cross section also can be given by

$$\sigma_b = \frac{M}{bh\varrho}\left[1 + \frac{y}{k(\varrho + y)}\right] \tag{3}$$

where ϱ is the radius of curvature of the centroidal axis, y is the distance from the centroidal axis to the given fiber, and k is the factor of rectangular cross section.

Because a combination of normal stress and bending stress must be taken into account in design using the interaction formula, the maximum axial stress σ_A (compressive stress) at the convex surface and the maximum axial stress σ_B (tensile stress) at the concave surface can be written as follows:

$$\sigma_A = \frac{P}{bh} - \frac{P(H + h/2)}{bh(R + h/2)}\left[1 + \frac{h/2}{k(R + h)}\right] \tag{4}$$

$$\sigma_B = \frac{P}{bh} - \frac{P(H + h/2)}{bh(R + h/2)}\left[1 - \frac{h/2}{kR}\right] \tag{5}$$

where R is the radius of curvature of the concave surface.

It can be shown that the radial stress is also created in a direction parallel to the radius of curvature (perpendicular to the grain) when curved LVL is subjected to a bending moment M,[8,12] shown in Fig. 2. The formula for computing the radial stress σ_R in member of constant rectangular cross section is:[8]

$$\sigma_R = -\frac{3M}{2bh(\varrho + y)}\left[1 - \left(\frac{y}{h/2}\right)^2\right] \tag{6}$$

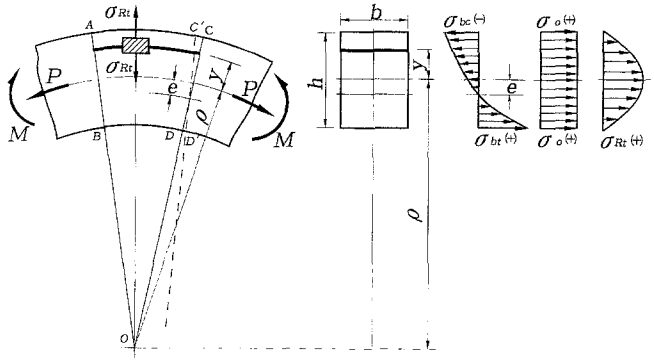

Fig. 2. Behavior of stress of curved LVL under loading. R, ϱ, P, h, see Fig. 1; M, bending moment; b, width; y, distance from the free portion to the centroidal axis; e, distance between the neutral axis and the centroidal axis; σ_0, normal stress; σ_{bt}, σ_{bc}, bending tensile and bending compressive stresses; σ_{Rt}, radial tensile stress

At the extreme surfaces ($y = \pm h/2$), $\sigma_R = 0$. The maximum radial stress σ_R occurs at the centroidal axis ($y = 0$), for which Eq. (6) can be given as

$$\sigma_R = \frac{3P(H + h/2)}{2bh(R + h/2)} \tag{7}$$

This σ_R is the tensile stress because the negative bending moment increases the radius of curvature and causes the member to become straighter. In contrast, a positive bending moment can resulted in the radial compressive stress.[8–12]

End-thrust loading (bending)

When the thrust load P that decreased the radius of curvature and caused the member to become more sharply curved is imposed at two ends of curved specimens with a span of L, shown in Fig. 1b, M (positive), σ_A (tensile stress) at the convex surface, σ_B (compressive stress) at the concave surface, and σ_R (compressive stress) at the centroidal axis can be written as follows:

$$M = P\left(H + \frac{h}{2}\right) \tag{8}$$

$$\sigma_A = -\frac{P}{bh} + \frac{P(H + h/2)}{bh(R + h/2)}\left[1 + \frac{h/2}{k(R + h)}\right] \tag{9}$$

$$\sigma_B = -\frac{P}{bh} + \frac{P(H + h/2)}{bh(R + h/2)}\left[1 - \frac{h/2}{kR}\right] \tag{10}$$

$$\sigma_R = -\frac{3P(H + h/2)}{2bh(R + h/2)} \tag{11}$$

Transverse loading (bending)

When the transverse concentrated load P that increased the radius of curvature and caused the member to become straighter is imposed at the convex surface of curved specimens with a support span of L, shown in Fig. 1c, M (negative), σ_A (compressive stress) at the convex surface, σ_B (tensile stress) at the concave surface, and σ_R (tensile stress) at the centroidal axis can be written as follows:

$$M = -\frac{P(L + (2H + h)\cot\theta)}{4} \tag{12}$$

$$\sigma_A = \frac{P\cot\theta}{2bh} - \frac{P(L + (2H + h)\cot\theta)}{4bh(R + h/2)}\left[1 + \frac{h/2}{k(R + h)}\right] \tag{13}$$

$$\sigma_B = \frac{P\cot\theta}{2bh} - \frac{P(L + (2H + h)\cot\theta)}{4bh(R + h/2)}\left[1 - \frac{h/2}{kR}\right] \tag{14}$$

$$\sigma_R = \frac{3P(L + (2H + h)\cot\theta)}{8bh(R + h/2)} \tag{15}$$

where θ is the support angle on the horizon at two support points of curved specimens under transverse bending (when the bent angle is γ, $\theta = \gamma/2$).

When the transverse concentrated load P also is imposed at straight specimens, σ_A at the upper surface and σ_B at the bottom surface can be written as follows:[5,6,13]

$$\sigma_A = \frac{3PL}{2bh^2} \tag{16}$$

$$\sigma_B = \frac{3PL}{2bh^2} \tag{17}$$

Experiments

Production of curved LVL

Curved LVL, structural members of chairs, were made from massion pine (*Pinus massoniana* Lamb.) and fast-growing poplar (*Populus euramericana* CV. I.).[1–3] The thickness and moisture content of veneers were 1.2mm and 8%–12%, respectively. The number of veneers was 19 or 21 so the curved LVL was maintained at 19 or 21mm thickness, respectively. Urea formaldehyde (UF) resin adhesives with a solid content of 61%–62% (mixed with the suitable ammonium chloride hardener and wheat flour extender) and the unit pressure of 1MPa supplied by a hydraulic press were used to make curved LVL with radiofrequency (RF) heating. The amount of UF adhesive applied by a hand roller to the veneers was 200g/m^2 (single spread).[1–3]

Types of specimens and fracture loads

Two specimens for each wood species were tested. Curved and straight specimens were cut from curved and straight parts of curved LVL that were structural members of chairs, respectively. Radii of curvature of curved specimens were 42, 56, 160, and 870mm. The bent angle of curved specimens with the radius of curvature of 42 or 56mm was 95°.

As shown in Fig. 1, three types of fracture load or conditions of loading (end-pull, end-thrust, and transverse) were applied to the curved specimens. The fracture load applied to straight specimens was transverse loading.[4–14]

Measurement of the maximum fracture loads

The maximum fracture loads of curved and straight specimens were tested under the different conditions of loading. The speed of testing was 5mm/min. Load–time diagrams were recorded. Failure types of the specimens were observed. In addition, moisture contents and densities of specimens of two wood species were measured. There were

Table 1. Dimensions of specimens and conditions of loading

R (mm)	*b* (mm)	*h* (mm)	*H* (mm)	*L* (mm)	*k*	*e* (mm)	*n*	*MC* (%)	*D* (g/cm^3)
End-pull loading (Massion pine)									
42	20.58(0.67)	20.75(0.75)	84	250	0.0136	0.707	6	15.51(0.84)	0.69(0.03)
56	23.00(0.00)	18.94(0.53)	80	250	0.0071	0.461	6	15.79(1.18)	0.73(0.04)
160	27.76(0.26)	20.56(0.65)	18	180	0.0012	0.208	10	14.58(0.66)	0.68(0.02)
End-thrust loading (Massion pine)									
42	20.42(0.61)	20.67(0.37)	84	250	0.0142	0.740	6	14.81(0.42)	0.70(0.05)
56	23.00(0.00)	19.00(0.54)	80	250	0.0071	0.463	6	16.32(1.65)	0.67(0.08)
160	27.75(0.25)	20.42(0.61)	18	180	0.0012	0.204	11	15.21(0.86)	0.74(0.05)
Transverse loading (Massion pine)									
42	19.93(0.32)	20.50(0.76)	90	265	0.0131	0.676	7	15.25(0.61)	0.72(0.08)
56	23.00(0.00)	18.58(0.78)	86	265	0.0068	0.444	6	14.75(0.68)	0.75(0.04)
160	27.77(0.27)	20.34(0.62)	20	192	0.0012	0.203	10	15.56(0.36)	0.73(0.05)
870	25.00(0.00)	20.93(1.27)	9	250	0.0001	0.044	12	15.39(0.58)	0.69(0.06)
ST	21.63(0.64)	20.53(1.18)	0	250	0	0	12	15.91(0.52)	0.71(0.05)
End-pull loading (fast-growing poplar)									
56	22.00(0.71)	18.54(0.86)	80	250	0.0062	0.402	5	13.79(0.21)	0.53(0.03)
End thrust loading (fast-growing poplar)									
56	23.00(0.00)	18.20(0.68)	80	250	0.0060	0.388	5	14.28(0.31)	0.55(0.06)
Transverse loading (fast-growing poplar)									
56	23.00(0.00)	18.50(0.60)	86	265	0.0063	0.408	5	15.21(0.48)	0.56(0.05)
870	25.06(0.29)	20.05(1.06)	9	250	0.0001	0.035	5	14.58(0.53)	0.57(0.03)
ST	22.14(0.53)	20.34(1.21)	0	250	0	0	5	15.06(0.32)	0.56(0.04)

R, radius of curvature of the concave surface; *b*, width; *h*, thickness; *H*, distance between the concave surface and the line of the loading or support points; *L*, support or imposition span; *k*, factor of the rectangular cross section; *e*, distance between the neutral axis and the centroidal axis; *n*, number of specimens; *MC*, moisture content; *D*, density; ST, straight laminated veneer lumber.
Values in parentheses represent standard deviations.

six specimens for each load test. The radius of curvature of the concave surface R, width b, thickness h, distance H between the concave and the line of the loading points, support span or imposition span L of the curved specimens, factor of the rectangular cross section k, distance e of the neutral axis deflected from the centroidal axis, number of specimens n used for each condition, moisture contents, and densities are shown in Table 1.

Calculation of stresses and analysis of failures

The maximum axial stresses occurring at both the convex and concave surfaces and the maximum radial stresses occurring at the centroidal axis of these specimens in loading tests were calculated by Eqs. (4), (5), (7), (9)–(11), and (13)–(17), respectively. To obtain suitable conditions of loading on curved LVL being used as structural members of furniture, the effects of radii of curvature and conditions of loading on stress distributions and failure types of curved LVL were analyzed, respectively.

Results and discussion

Stresses and their distributions

Table 2 and Figs. 3, 4, and 5 show the maximum axial stresses at both the convex and concave surfaces, the maximum radial stresses at the centroidal axis, the moisture contents, and the densities of curved and straight specimens, respectively.

From Table 2 and Figs. 3 and 4, it is apparent that absolute values of the maximum axial stresses σ_A occurring at the convex surface were smaller than those σ_B that occurred at the concave surface under three conditions of loading. With end-thrust loading, when the curved member is subjected to both bending and axial normal compression, the combination of the normal compressive stresses and the bending tensile stresses caused by bending moment results in a smaller absolute value of stress on the tension side (convex) than on the compression side (concave).[12] With end-pull or transverse loading, when the curved member is subjected to both bending and axial normal tension, the combination of the normal tensile stresses and the bending compressive stresses caused by bending moment results in a smaller absolute value of stress on the compression side (convex) than on the tension side (concave) as well. This is due to the fact that the neutral axis deflects from the centroidal or symmetrical axis into the half section between the centroidal axis and the concave surface when curved LVL specimens are subjected to a bending moment M,[8,9,12] as shown in Fig. 2. However, differences between σ_A and σ_B decreased with an increase in the radius of curvature of the LVL.

Distributions of radial stress σ_R created in the direction of the radius of curvature are parabolic. At both convex and concave surfaces, $\sigma_R = 0$. The maximum radial stresses

Table 2. Fracture loads and stresses under three conditions of loading

R (mm)	P (Kgf)	Δ (mm)	σ_A (MPa)	σ_B (MPa)	σ_R (MPa)
End-pull loading (Massion pine)					
42	70.99(3.49)	12.36(5.13)	−38.57(4.23)	54.22(5.38)	4.51(0.34)
56	80.75(4.89)	14.94(3.51)	−46.19(2.95)	60.18(3.66)	3.81(0.21)
160	361.34(66.05)	2.94(1.31)	−48.89(8.81)	60.76(9.48)	1.58(0.29)
End-thrust loading (Massion pine)					
42	100.95(7.32)	−16.75(2.60)	52.64(3.48)	−69.45(4.57)	−6.15(0.41)
56	98.92(12.75)	−17.51(3.17)	55.97(4.64)	−72.99(5.87)	−4.63(0.41)
160	556.52(99.82)	−3.72(1.29)	78.25(9.69)	−84.77(9.31)	−2.44(0.61)
Transverse loading (Massion pine)					
42	58.21(6.99)	−11.29(1.48)	−40.87(6.05)	54.75(7.84)	3.24(0.42)
56	64.50(11.50)	−12.89(2.74)	−50.23(7.84)	62.67(9.02)	2.67(0.41)
160	201.54(27.42)	−4.29(1.83)	−56.12(7.04)	62.88(7.88)	1.02(0.13)
870	249.19(46.21)	−8.74(1.01)	−84.00(9.76)	85.35(9.94)	0.25(0.04)
ST	248.96(30.47)	−6.17(1.30)	−86.13(8.52)	86.13(8.52)	0
End-pull loading (fast-growing poplar)					
56	87.98(6.59)	25.43(9.88)	−61.34(8.46)	78.54(9.95)	4.69(0.46)
End-thrust loading (fast-growing poplar)					
56	66.12(13.51)	−49.18(9.92)	42.70(8.72)	−54.38(9.98)	−3.44(0.71)
Transverse loading (fast-growing poplar)					
56	76.23(10.49)	−23.01(1.58)	−62.54(4.70)	77.02(6.20)	3.31(0.34)
870	228.59(28.79)	−10.06(1.63)	−84.23(6.01)	85.52(6.08)	0.24(0.02)
ST	234.15(16.51)	−8.12(1.30)	−87.09(7.64)	87.09(7.64)	0

R, ST, see in Table 1; P, maximum load; Δ, deformation of imposition span L under end-pull and end-thrust loading or deformation of distance H (Table 1) under transverse loading; σ_A, σ_B, maximum axial stresses at the convex and concave surfaces; σ_R, maximum radial stress at the centroidal axis.
Values in parentheses represent standard deviations.

occurred at the centroidal axis. With end-pull or transverse loading the bending moment that reduced the initial curvature of curved LVL induced the radial tensile stress. Conversely, with end-thrust loading the bending moment that increased the initial curvature induced the radial compressive stress.

Failure types

Figures 6, 7, and 8 show failures of curved specimens of two wood species under different loading tests. Figure 9 shows relations between load and time according to the load–time diagrams recorded.

With end-pull testing (Fig. 6) of curved specimens of two wood species, there were mainly splitting failures parallel to the glue-line. First, slight splitting failures occurred at glue-lines close to the concave surface. Then, large splitting failures were created at glue-lines near the centroidal axis. Finally, the splitting extended from the centroidal axis to both the concave and convex surfaces. These splitting failures were more significant on the tensile side than on the compression side.

With end-thrust testing (Fig. 7) of curved specimens of two wood species, there were more fibrous fractures on the tensile side and crushing failures on the compression side closest to the concave surface. Fibrous fractures of curved specimens were larger in fast-growing poplar than in massion pine.

With transverse testing (Fig. 8), curved specimens of massion pine created mainly splitting failures at glue-lines near the centroidal axis. Finally, this splitting failure extended throughout the cross section, and it was significant in the tensile side. In contrast, for curved specimens of fast-growing poplar, fibrous fractures occurred mainly on the tensile side. However, with this condition of loading there were obvious fibrous fractures on the tensile side of straight specimens of two wood species.

According to the analysis of stress distributions stated above, the failures observed under different conditions of loading can be explained as follows. The splitting failure in the glue-line mainly resulted from the maximum tensile radial stress σ_R and occurred at the centroidal axis, because the negative bending moment increases the radius of curvature and causes the member to become straighter under the end-pull and transverse testing of curved specimens.[8–15] Moreover, when the maximum compressive and tensile stresses caused by bending occurred in both surfaces, there was a tendency for the upper veneer of the piece to slide along the lower veneer, and a horizontal shear stress occurred along every glue-line in the thickness; hence the maximum horizontal shear stress occurred in the neutral axis.[13,14,16–18] The maximum horizontal shear stress resulted also in a splitting failure. When the dimensions (width and

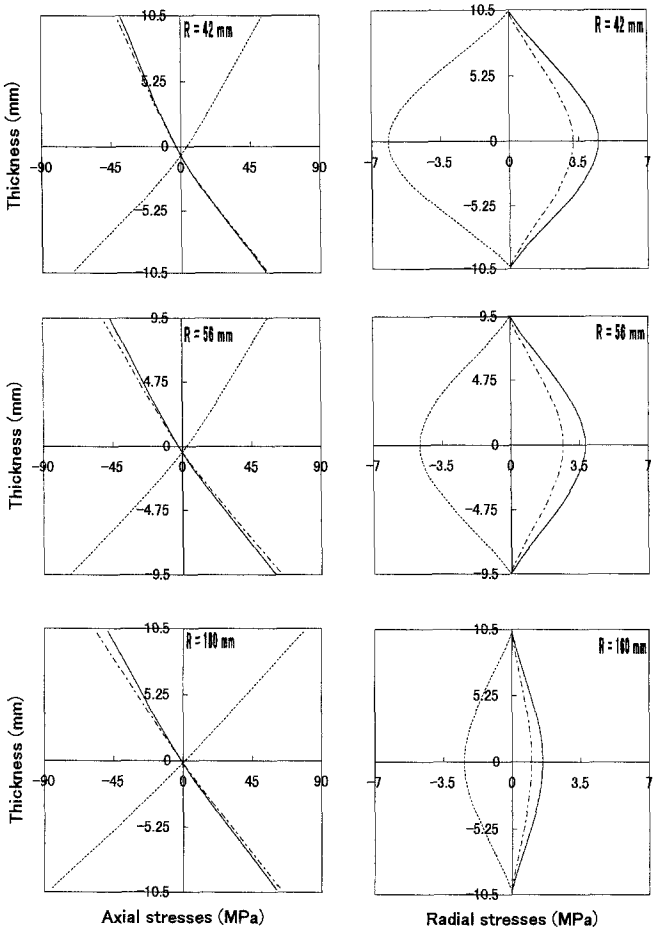

Fig. 3. Distribution of stress of curved LVL of massion pine under loading. *Solid line*, end-pull loading; *dotted line*, end-thrust loading; *long-short dashes*, transverse loading. Positive and negative values in the thickness represent the convex and concave sides, respectively

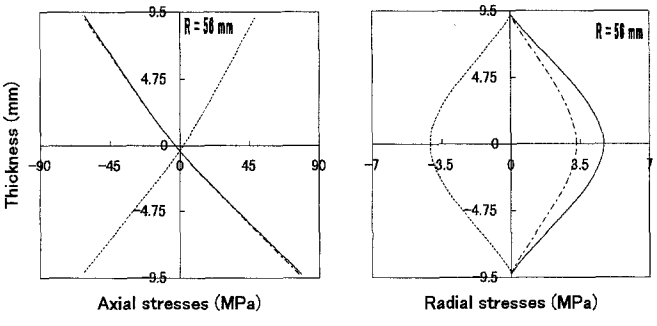

Fig. 4. Distribution of stress of curved LVL of fast-growing poplar under loading. *Solid line*, end-pull loading; *dotted line*, end-thrust loading; *long-short dashes*, transverse loading. See Fig. 3

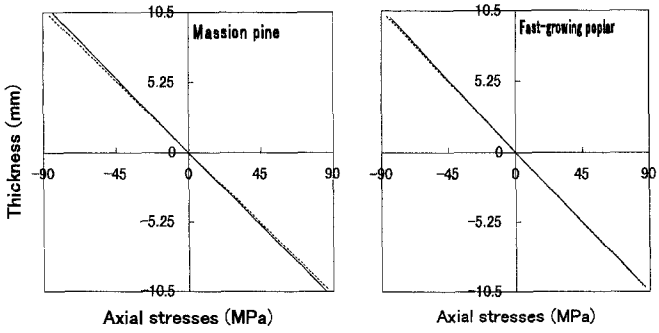

Fig. 5. Distribution of stress of LVL under transverse loading. *Solid line*, curved LVL with the radius of curvature of 870 mm; *dotted line*, straight LVL. See Fig. 3

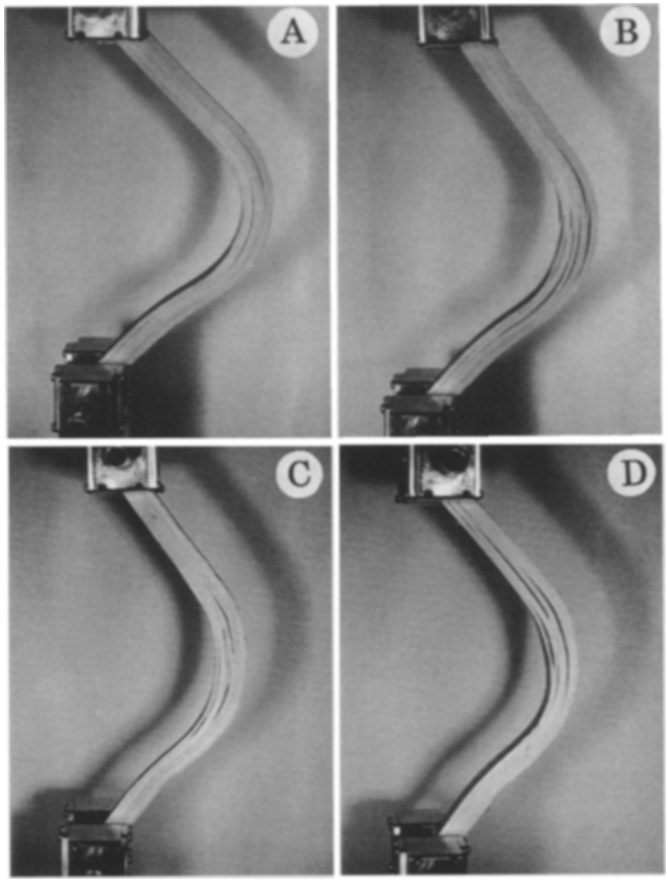

Fig. 6. Types of failure of curved LVL under end-pull loading. **A,B** Massion pine. **C,D** Fast-growing poplar

thickness) of the cross section are much smaller than the length, the effect of a horizontal shear stress on failure can be ignored.[19] In contrast, the fibrous fracture and crushing failure resulted from the maximum axial tensile stress (σ_A with end-thrust testing or σ_B with transverse testing) and the maximum axial compressive stress (σ_B with end-thrust testing), respectively.

The load-time diagrams (Fig. 9) recorded in three conditions of loading show that fractures of specimens of two wood species occurred in a different manner. Massion pine specimens had failures with small deformations (Δ in Table 2) and the failures occurred quickly, whereas fractures of fast-growing poplar specimens obviously were accompanied by rather large deformations (Δ in Table 2) and required more time.

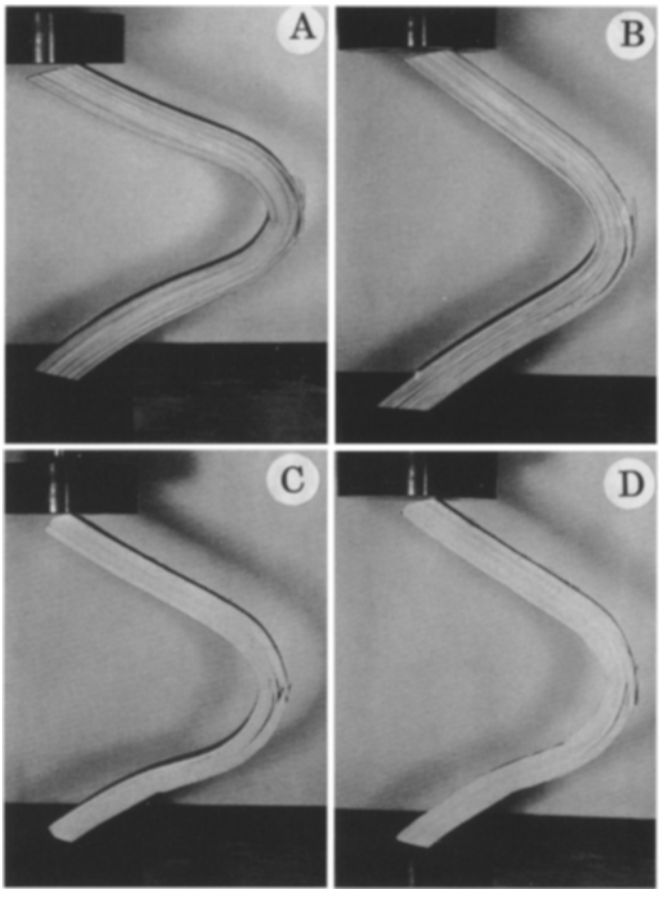

Fig. 7. Types of failure of curved LVL under end-thrust loading. **A,B** Massion pine. **C,D** Fast-growing poplar

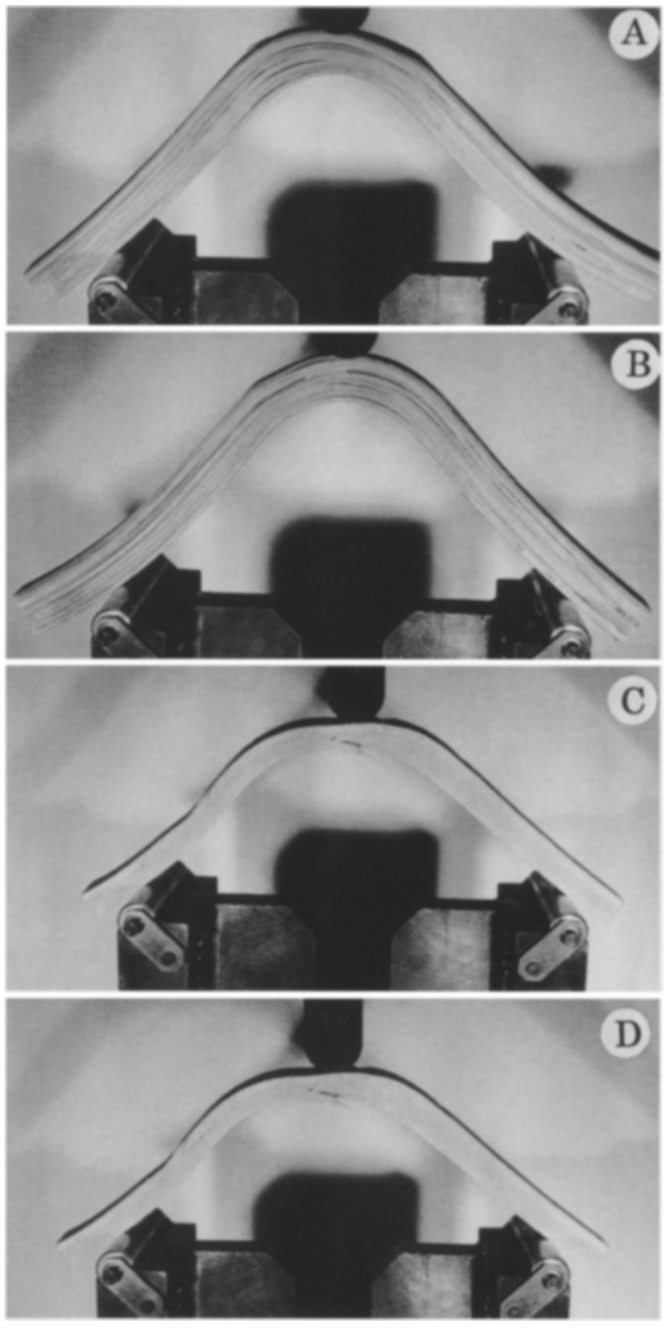

Fig. 8. Types of failure of curved LVL under transverse loading. **A,B** Massion pine. **C,D** Fast-growing poplar

Relations between stresses and radii of curvature

The relations between absolute values of stresses (σ_A, σ_B, σ_R) and the radii of curvature of curved LVL can be seen in Table 2. The results show that absolute values of σ_A and σ_B significantly increased with an increase in the radius of curvature under three conditions of loading. In contrast, absolute values of σ_R decreased with an increase in the radius of curvature.

Moreover, the differences between σ_A and σ_B decreased with an increase in the radius of curvature. Curved specimens with a large radius of curvature or straight specimens indicated the same values for σ_A and σ_B. For example, when the radius of curvature R is 870 mm, the absolute value was no significant difference between σ_A (−84.00 MPa) and σ_B (85.35 MPa) computed by Eqs. (13) and (14) of curved specimens of massion pine with transverse loading. They were almost similar to the results of σ_A (−84.67 MPa) and σ_B (84.67 MPa) computed by Eqs. (16) and (17) for straight specimens. Curved specimens of fast-growing poplar with the radius of curvature of 870 mm have results similar with transverse loading: σ_A is −84.23 MPa and σ_B is 85.52 MPa computed by Eqs. (13) and (14); σ_A is −84.87 MPa and σ_B is 84.87 MPa computed by Eqs. (16) and (17) for straight specimens.

From the theory of strength of materials, the above results can be explained by the fact that pre-stress is induced when laminations are bent to curved forms. Although much of these stresses are quickly relieved or decreased in time through relaxation, some remain and tend to reduce the strength of a curved member.[12,20–23] Therefore, the axial stresses in curved laminated members are less than those in straight members.[12] In addition, because the distance (e) that the neutral axis deflects from the centroidal or symmetrical axis into the half of concave section decreased with an increase in the radius of curvature of curved specimens,

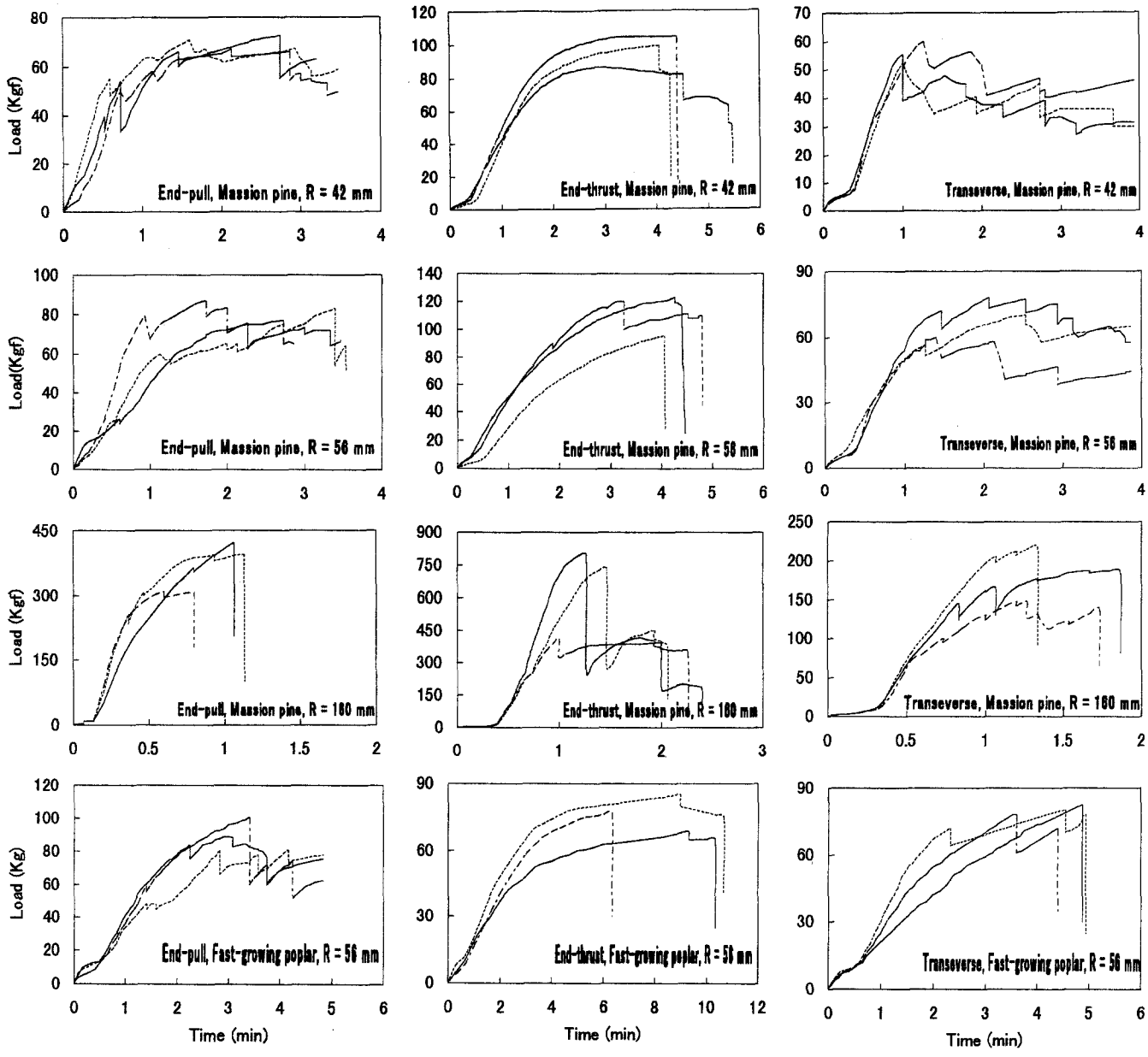

Fig. 9. Load–time relations of curved LVL under three conditions of loading. *Solid line*, *dotted line*, *long-short dashes*, three typical specimens. The speed of testing was 5 mm/min

these residual stresses also decreased with an increase in the radius of curvature.

Effects of conditions of loading on stress and failure

From the results of Table 2 and Figs. 3 and 4, the relations between absolute values of stresses (σ_A, σ_B, σ_R) and conditions of loading can be obtained under different radii of curvature of curved LVL of two wood species. The results show that absolute values of σ_A, σ_B, and σ_R of curved LVL of massion pine were larger with end-thrust loading than with end-pull or transverse loading. In contrast, absolute values of σ_A and σ_B of curved LVL of fast-growing poplar were smaller with end-thrust loading than with end-pull or transverse loading. The latter finding is similar to the results of Takami (red lauan, harunire),[6] Ikuta (ezomatsu, mizunara),[13,14] and Kenmochi (beech).[24] The differences between the two wood species were due to the difference in their structures and properties. On the other hand, because massion pine contains large amounts of oleoresin that can influence the adhesive property of the glue-line,[1–3] splitting failures were created easily. However, absolute values of σ_A and σ_B of curved LVL of two wood species with end-pull loading were similar to those with transverse loading.

Because there were different distributions of stresses σ_A, σ_B, and σ_R under three conditions of loading, different types of failure occurred. With end-thrust loading, even though

absolute values of σ_R (radial compressive stress) of curved LVL of massion pine were larger than those with end-pull and transverse loading, splitting failures were not created because the positive bending moment decreased the radius of curvature and caused the member to become more sharply curved. Results of fibrous fractures and crushing failures were due to acting of the maximum axial tensile and axial compressive stress, respectively. In contrast, because the negative bending moment increased the radius of curvature and caused the member to become straighter, radial tensile stress σ_R resulted in splitting failures with end-pull and transverse loading.

In addition, it is clear that curved LVL of massion pine were more suitable under conditions of loading that decrease the radius of curvature (e.g., end-thrust loading) than under conditions of loading that increase the radius of curvature (e.g., end-pull and transverse loading). In contrast, curved LVL of fast-growing poplar were suitable under not only conditions of loading that increase the radius of curvature but also conditions of loading that decrease the radius of curvature. Therefore, to ensure the appropriate use of curved LVL made from two wood species as structural members of furniture, it is important to consider the suitable direction of loading on curved LVL.

Conclusions

In curved LVL of massion pine and fast-growing poplar, absolute values of the maximum axial stresses (the combination of the axial normal stress and the maximum axial bending stress) (σ_A) occurring at the convex surface were smaller than those (σ_B) at the concave surface under end-pull, end-thrust, and transverse loadings. Differences between σ_A and σ_B decreased with an increase in the radius of curvature of LVL. With end-pull loading of curved specimens of two wood species, there were mainly splitting failures at glue-lines near the centroidal axis. With end-thrust loading there were more fibrous fractures on the tensile side and crushing failures on the compression side closest to the concave surface. Fibrous fractures of curved specimens were larger in fast-growing poplar than in massion pine. With transverse loading, curved specimens of massion pine suffered mainly splitting failures. In contrast, for curved specimens of fast-growing poplar and straight specimens of two wood species, fibrous fractures occurred mainly on the tensile side.

Absolute values of σ_A and σ_B significantly increased with an increase in the radius of curvature under three conditions of loading. In contrast, absolute values of the maximum radial stress (σ_R) at the centroidal axis decreased with an increase in the radius of curvature. Absolute values of σ_A, σ_B, and σ_R of curved LVL of massion pine were larger under end-thrust loading than under end-pull and transverse loading. Conversely, absolute values of σ_A and σ_B of curved LVL of fast-growing poplar were small with end-thrust loading. However, absolute values of σ_A and σ_B of curved LVL of two wood species with end-pull loading were almost similar to those with transverse loading.

References

1. Wu ZH, Furuno T, Zhang BY (1997) Temperature properties of curved laminated veneer lumber during hot pressing with radio frequency heating. Mokuzai Gakkaishi 43:847–854
2. Wu ZH, Furuno T, Zhang BY (1997) Strength properties of curved laminated veneer lumber made from fast-growing species (in Japanese). In: Abstracts of 9th annual meeting of Chugoku Shikoku branch of the Japan Wood Research Society, Tottori, pp 44–45
3. Wu ZH, Furuno T, Zhang BY (1998) Properties of curved laminated veneer lumber made from fast-growing species with radio frequency heating for use in furniture. J Wood Sci 44:275–281
4. Nakahara I (1994) Strength of materials (in Japanese). Yokendo, Tokyo, pp 109–124
5. Utoguchi T (1996) Strength of materials (in Japanese). Shoukabou, Tokyo, pp 306–322
6. Takami I (1978) Strength of circular-curved laminated wood (in Japanese). Mokuzai Gakkaishi 24:541–545
7. Mori K, Hata S, Ohira A (1985) Strength properties of glued laminated timber used for 19 years (in Japanese). Wood Ind 40(5):24–29
8. German G (1973) Wood engineering. Southern Forest Products Association, Upton, Louisiana, pp 188–256
9. Wu ZH (1990) Calculation of bending stress in wood bending forming members (in Chinese). Building Wood-based Panels 4:10–14
10. Japan Construction Research Society (1995) Standard for structural design of timber structures (in Japanese). Gihoudo, Tokyo, pp 40–42, 222–226
11. Japan Construction Research Society (1995) Structural design notes for timber structures (in Japanese). Sanbi, Tokyo, pp 307–317
12. American Institute of Timber Construction (1985) Timber construction manual. Wiley, New York, pp 74–75, 197–201, 217–218
13. Ikuta H (1983) Radial stresses in curved glued-laminated timbers. T. (in Japanese). Mokuzai Gakkaishi 29:500–506
14. Ikuta H (1984) Radial stresses in curved glued-laminated timbers. II. (in Japanese). Mokuzai Gakkaishi 30:720–726
15. Hashimoto K, Narita J (1989) Illustrating joint construction for woodworking (in Japanese). Rikogakusha, Tokyo, pp 60–62
16. Ebihara T (1981) Shear properties of laminated veneer lumber (LVL) (in Japanese). Mokuzai Gakkaishi 27:788–794
17. Suzuki N, Sasaki H (1987) Calculation of fracture toughness of bending specimens with central crack in a sliding mode by finite-element method. I. (in Japanese). Mokuzai Gakkaishi 33:182–187
18. Kollmann FFP, Kuenzi EW, Stamm AJ (1975) Principles of wood science and technology. II. Wood based material. Springer, Berlin, pp 260–262
19. Asano I (1965) Study on the bending of the glued laminated wood-beams (in Japanese). Bull For Faculty Agric Sci Nagoya Univ 4:1–49
20. Sasaki Y, Tsuzuki K, Adachi K (1991) Stress analyses of curved laminated-wood beams considering the residual stresses. I. (in Japanese). Mokuzai Gakkaishi 37:661–667
21. Miyatake A (1990) Residual stresses in curved laminated timber (in Japanese). Wood Ind 45(10):19–22
22. Wangaard FF, Woodson GE, Murray MR (1968) Species response to pre-stress in curved laminated wood beams. For Prod J 18(1):49–56
23. Woodson GE, Wangaard FF (1969) Effect of forming stresses on the strength of curved laminated beams of loblolly pine. For Prod J 19(3):47–58
24. Kenmochi H (1987) Cyclopedia for furniture (in Japanese). Asakura-shoten, Tokyo, pp 472–474